nature climate change

SUPPLEMENTARY INFORMATION

DOI: 10.1038/NCLIMATE1890

PROJECTED INCREASE IN TROPICAL CYCLONES NEAR HAWAII

Hiroyuki Murakami[1, 2], Bin Wang[2], Tim Li[2], and Akio Kitoh[1]

[1]Meteorological Research Institute, Tsukuba, Ibaraki, Japan

[2]Department of Meteorology and International Pacific Research Center,

University of Hawaii at Manoa, Honolulu, Hawaii 96822, USA

Supplementary Methods

Model

The model used in this study is the Meteorological Research Institute Atmospheric General Circulation Model (MRI-AGCM) version 3.1 (v3.1; ref. 29) and 3.2 (v3.2; ref. 30). The MRI-AGCM was developed from the Japan Meteorological Agency (JMA) Global Numerical Weather Prediction (NWP) model[31]. The dynamical core of the model uses hydrostatic primitive equations and is solved using a spectral transform method with spherical harmonics. The model adopts a semi-Lagrangian scheme[32]. The model simulations are run at a horizontal resolution of T_L959 (equivalent to a 20-km mesh) or T_L319 (60-km-mesh). There are 60 vertical layers (top at 0.1 hPa) for v3.1 and 64 layers (top at 0.01 hPa) for v3.2.

Although the two versions share the same dynamical core, some physical processes differ slightly between them (Supplementary Table 1). Details are also available in ref. 30. V3.1 is equipped with a prognostic Arakawa–Schubert (AS) cumulus convection scheme[33–34]. In this scheme, multiple convective updrafts with different heights are explicitly calculated within a single grid cell, with each updraft represented as a simplified entraining plume. In

v3.2, a new cumulus scheme, named the "Yoshimura scheme (YS)[35] after a model developer at the MRI, has been introduced. The YS scheme is based on the Tiedtke[36] scheme with some modifications. In the original Tiedtke scheme, only a single convective updraft is calculated within each grid cell, but this updraft is represented as a more detailed entraining and detraining plume than updrafts in the AS scheme. The YS scheme accounts for multiple detailed entraining and detraining plumes by interpolating two convective updrafts with different rates of turbulent entrainment and detrainment. Thus, the new cumulus convection scheme combines the advantages of the AS and the original Tiedtke schemes. In v3.2, the Kain–Fritsch (KF)[37] cumulus convection scheme is also available. The KF scheme is a mass flux scheme in which the cloud base mass flux is determined by the amount of convective available potential energy (CAPE) in the environment that needs to be removed.

Experimental settings

A so-called "time-slice" method[38] is applied, in which the high-resolution AGCM is forced by setting the lower boundary conditions to prescribed SSTs. In this study we conducted 5 present-day climate simulations and 11 future climate projections (Supplementary Table 2), with differences in model version (v3.1 and v3.2), cumulus convection scheme (3 different schemes), spatial pattern of tropical SST changes (4 different SST distributions, as described below), and resolution (20- and 60-km mesh). This approach allows us to address the uncertainties in future projections of TC activity caused by these differences.

The present-day simulations are prescribed with observed monthly mean SST and sea ice concentration (SIC) [i.e., an Atmospheric Model Intercomparison Project (AMIP)-style simulation] during 1979–2003 from the Hadley Centre Global Sea Ice and Sea Surface

Temperature dataset (HadISST1[39]), along with the monthly climatology of sea ice thickness from ref. 40. Concentrations of greenhouse gases (GHG; e.g., CO_2, CH_4, N_2O, and CFCs) are set to the observed global mean, annual-mean values, changing from year to year. Aerosols for the present-day simulations using v3.2 are obtained from a present-day simulation with a prototype version of the MRI-Earth System Model (ESM1[35]), in which the historical emission flux of anthropogenic SO_2, invariant SO_2 flux from non-eruptive volcanoes, and the surface emission inventories for carbonaceous aerosols are prescribed, while those for simulations with v3.1 are obtained from a previous version of the MRI aerosol chemical transport model[41].

The main target for the future projections is the last quarter of the 21st century (2075–2099). For the future projection, four different projections of future SST are prescribed, each with a different spatial SST anomaly pattern (Supplementary Figure 4). One of these patterns is the multi-model ensemble mean SST computed from projected future changes obtained from the 18 World Climate Research Programme's Coupled Model Inter-comparison Project phase 3 (CMIP3)[22] models under the Special Report on Emission Scenarios (SRES) A1B scenario[14] (hereafter referred to as MME SST; refs 1–3). Note that we did not use the raw time series of the multi-model ensemble mean as the future SST because the averaging among the models acts to smooth out year-to-year variability of SST and excludes ENSO. In addition, if future SST fields projected by the CMIP3 models are used directly, it is difficult to evaluate future changes from the present-day simulations using the observed SST because of large biases in CMIP3 models in their present-day simulations (i.e., C20C experiments). To avoid these problems, MME SST for the future was estimated following the method described in ref. 42 (see the schematic diagram in Supplementary Figure 5). First, for each grid cell, observed SST is decomposed into a trend (PDTR) component and an inter-annual variation (PDIV) for

the 25 years from 1979 to 2003. Second, the same decomposition was applied to the ensemble mean of the CMIP3 models, thereby obtaining the future trend (GWTR) and inter-annual variation for the 25 years from 2075 to 2099 (GWIV). The average value of SST for each present-day (C20C) and future (SRES A1B) experiment was also calculated so that mean future change (GWDT) was computed. Finally, the future anomaly was reconstructed by combining GWDT, GWTR and PDIV; the MME SST for the future was then created by superposing the anomaly on the detrended observed mean SST for the period 1979−2003. Note that here the amplitude and phase of the inter-annual variation are assumed to be conserved in the future setting.

The other three SST fields are created using a cluster analysis (hereafter referred to as C1–C3 SSTs; refs 1 and 3), because we assumed future changes in tropical cyclone activity are sensitive to future changes in the spatial pattern of tropical SST. The procedure for the cluster analysis is as follows[1]:

(1) For each CMIP3 model, a mean future change in SST is computed by subtracting the 1979–2003 mean SST from the 2075–2099 mean SST.

(2) The computed mean future change in SST is normalised by dividing by the tropical mean (30°S–30°N) future change in SST.

(3) The normalised value for each model is subtracted from the multi-model ensemble mean of the normalised value.

(4) The inter-model pattern correlation r of the normalised values is computed for each pair of models.

(5) Norms (or distances) are defined as $2 \times (1 - r)$ for each model, and the cluster analysis is performed using these norms. A small distance between two models indicates that

they share similar spatial patterns in future changes in tropical SST. Clustering is based on the *Single-linkage* (or minimum-distance) method[43], in which the smallest distance between two models (or groups) is joined step-by-step. When the final three groups are bounded, the clustering procedure is terminated.

Only three cluster groups are identified (Supplementary Figure 6), because a greater number of groups would increase the risk that a single outlier model would dominate the results. After identifying the CMIP3 models for each cluster, the future SST is computed using the same procedure as described above for the MME SST for the future. Future changes in mean SST for the three cluster groups are shown in Supplementary Figure 4b–d. C1 shows less warming over the central Pacific relative to other clusters, so that the spatial variation in the tropics is small. C2 is similar to MME SST, but with greater warming in the Indian Ocean than the other prescribed SSTs. C3 has the largest spatial variation in the tropics of all of the prescribed SSTs, and shows relatively large warming of SST in the tropical western Pacific and subtropical central Pacific.

The GHG concentrations for the future period are based on the SRES A1B scenario[14], while aerosols are obtained from the result of a future projection based on the Intergovernmental Panel on Climate Change (IPCC) A1B scenario using the MRI-ESM1 for the projections with v3.2 (using the chemical transport model[41] for the projections with v3.1).

In addition to the 11 future experiments, an additional idealized experiment that assumes a globally uniform SST change of +1.83°C (the global mean SST increase between 1979–2003 and 2075–2099 based on the CMIP3 MME SST) is also conducted for comparison with the experiments in which SST changes vary spatially. In this experiment, other settings such as GHG concentrations are exactly the same as in the other future experiments. This

experiment was conducted using the 60-km-mesh v3.2 model with the YS cumulus convection scheme.

Tropical cyclone detection method

Model-generated TCs are detected using the method described by ref. 19, in which criteria are set for a given model configuration to ensure that the present-day annual mean TC number in the eastern Pacific domain matches that observed (about 16.7 per year for the period 1979–2003 based on the dataset provided by Unisys[23]). The criteria to be optimized are 1) the magnitude of the maximum relative vorticity at 850 hPa, and 2) the temperature deviations at 300, 500, and 700 hPa for detecting warm core structure in a TC. Other than these criteria, three fixed criteria independent of the experiments are also applied: 3) the maximum wind speed at 850 hPa should be higher than that at 300 hPa (to exclude extra-tropical cyclones), 4) the genesis position should be over the ocean, and 5) the duration should exceed 36 hours. To avoid dependency of the results on the above criteria, the optimized values of criteria 1 and 2 are slightly changed to generate 25 other sets of the detection criteria, resulting in the annual mean TC number varying by ±10%. Each simulation has 26 sets of detection results in total, and their ensemble mean is evaluated to represent the simulation result.

References

29. Mizuta, R. *et al.* 20-km-mesh global climate simulations using JMA-GSM model –mean climate states–. *J. Meteor. Soc. Japan* **84,** 165–185 (2006).

30. Mizuta, R. *et al.* Climate simulations using MRI-AGCM3.2 with 20-km grid. *J. Meteor. Soc. Japan* **90A,** 233–258 (2012).

31. JMA. Outline of the operational numerical weather prediction at the Japan Meteorological Agency (Appendix to WMO technical progress report on the global data-processing and forecasting system and numerical weather prediction). *Japan Meteorological Agency* 194 pp. [Available online at http://www.jma.go.jp/jma/jma-eng/jma-center/nwp/outline-nwp/index.htm] (2007).

32. Yoshimura, H. & Matsumura, T. A semi-Lagrangian scheme conservative in the vertical direction. *CAS/JSC WGNE Research Activities in Atmospheric and Oceanic Modeling* **33,** 0319–0320 (2003).

33. Arakawa, A. & Schubert, W. H. Interaction of cumulus cloud ensemble with the large-scale environment. Part I. *J. Atmos. Sci*. **31,** 674–701 (1974).

34. Randall, D. & Pan, D. -M. Implementation of the Arakawa-Schubert cumulus parameterization with a prognostic closure. The representation of cumulus convection in numerical models. *Meteor. Monogr., Amer. Meteor. Soc*. **46,** 137–144 (1993).

35. Yukimoto, S. *et al.* Meteorological Research Institute-Earth System Model version 1 (MRI-ESM1) – Model Description –. *Tech. Rep. Meteor. Res. Inst.* **64,** 88pp. [available at http://www.mri-jma.go.jp/Publish/Technical/DATA/VOL_64/index.html] (2011).

36. Tiedtke, M. A comprehensive mass flux scheme for cumulus parameterization in large-scale models. *Mon. Wea. Rev*. **117,** 1779–1800 (1989).

37. Kain, J. S. & Fritsch, J. M. A one-dimensional entraining/detraining plume model and its application in convective parameterization. *J. Atmos. Sci.* **47,** 2784–2802 (1990).

38. Bengtsson, L., Botzet, M. & Esch, M. Will greenhouse gas-induced warming over the next 50 years lead to higher frequency and greater intensity of hurricanes? *Tellus* **48A,** 57–73 (1996).

39. Rayner, N. A. *et al.* Global analysis of sea surface temperature, sea ice, and night marine air temperature since the late nineteenth century. *J. Geophys. Res*. **108,** 4407 (2003).

40. Bourke, R. H. & Garrett, R. P. Sea ice thickness distribution in the Arctic Ocean. *Cold Regions Sci. and Tech.* **13,** 259–280 (1987).

41. Tanaka, T. Y. *et al.* MASINGAR, a global tropospheric aerosol chemical transport model coupled with MRI/JMA98 GCM: Model description. *Pap. Meteor. Geophys.* **53,** 119–138 (2003).

42. Mizuta, R., Adachi, Y., Yukimoto, S. & Kusunoki, S. Estimation of the future distribution of sea surface temperature and sea ice using the CMIP3 multi-model ensemble mean. *Tech.*

Reports of the MRI **56,** 28pp. [available online at http://www.mri-jma.go.jp/Publish/Technical/DATA/VOL_56/56.html] (2008).

43. Wilks, D. S. Cluster analysis. In: Statistical methods in the atmospheric sciences, Wilks D.S (ed), 2nd edn. *Academic Press* London, pp 594–562 (2006).

44. Smith, R N. B. A scheme for predicting layer clouds and their water content in a general circulation model. *Quart. J. Roy. Meteor. Soc*. **116,** 435–460 (1990).

45. Tiedtke, M. Representation of clouds in large-scale models. *Mon. Wea. Rev*. **121,** 3040–3061 (1993).

46. Shibata, K. & Aoki, T. An infrared radiative scheme for the numerical models of weather and climate. *J. Geophys. Res*. **94,** 14923–14943 (1989).

47. Shitaba, K. & Uchiyama, A. Accuracy of the delta-four-stream approximation in inhomogeneous scattering atmospheres. *J. Meteor. Soc. Japan* **70,** 1097–1109 (1992).

48. Iwasaki, T., Yamada, S. & Tada, K. A parameterization scheme of orographic gravity wave drag with the different vertical partitioning, part 1: Impact on medium range forecast. *J. Meteor. Soc. Japan* **67,** 11–41 (1989).

49. Hirai, M. *et al.* Development and validation of a new land surface model for JMA's operational global model using the CEOP observation dataset. *J. Meteor. Soc. Japan* **85A,** 1–24 (2007).

50. Mellor, G. L. & Yamada, T. A hierarchy of turbulence closure models for planetary boundary layers. *J. Atmos. Sci.* **31,** 1791–1806 (1974).

Supplementary Table

SUPPLEMENTARY TABLE 1 Comparison of physical processes between the two versions of MRI-AGCM.

Model version	MRI-AGCM3.1 (v3.1)[29]	MRI-AGCM3.2 (v3.2)[30]
Cumulus convection	Prognostic Arakawa-Schubert (AS)[33–34]	Yoshimura (YS)[35], Kain-Fritsch (KF)[37]
Cloud	Smith[44]	Tiedtke[45]
Radiation	Shibata and Aoki[46], Shibata and Uchiyama[47]	JMA[31]
Gravity wave drag	Iwasaki et al.[48]	
Land surface	Hirai et al.[49]	
Boundary layer	Mellor and Yamada (level 2)[50]	
Aerosol (direct)	Sulphate aerosol	Five species

SUPPLEMENTARY TABLE 2 Experiment design.

No	Model Version	Cumulus Convection Scheme	Sea Surface Temperature	Grid Size (km)
		Present-day Simulations for 1979–2003 (25 years)		
1	v3.1	Arakawa-Schubert (AS)	Observation HadISST1[a]	20
2	v3.1	Arakawa-Schubert (AS)	Observation HadISST1	60
3	v3.2	Yoshimura (YS)	Observation HadISST1	20
4	v3.2	Yoshimura (YS)	Observation HadISST1	60
5	v3.2	Kain-Fritsch (KF)	Observation HadISST1	60
		Future Projections for 2075–2099 (25 years)		
1	v3.1	Arakawa-Schubert (AS)	CMIP3[b] MME[c] (MME)	20
2	v3.1	Arakawa-Schubert (AS)	CMIP3 MME (MME)	60
3	v3.2	Yoshimura (YS)	CMIP3 MME (MME)	20
4	v3.2	Yoshimura (YS)	CMIP3 MME (MME)	60
5	v3.2	Yoshimura (YS)	Cluster 1 (C1)	60
6	v3.2	Yoshimura (YS)	Cluster 2 (C2)	60
7	v3.2	Yoshimura (YS)	Cluster 3 (C3)	60
8	v3.2	Kain-Fritsch (KF)	CMIP3 MME (MME)	60
9	v3.2	Kain-Fritsch (KF)	Cluster 1 (C1)	60
10	v3.2	Kain-Fritsch (KF)	Cluster 2 (C2)	60
11	v3.2	Kain-Fritsch (KF)	Cluster 3 (C3)	60

[a]Observational data by the Hadley Centre of Met Office, United Kingdom[39].

[b]Coupled Model Intercomparison Project 3[22].

[c]Multi-Model Ensemble.

Supplementary Figure

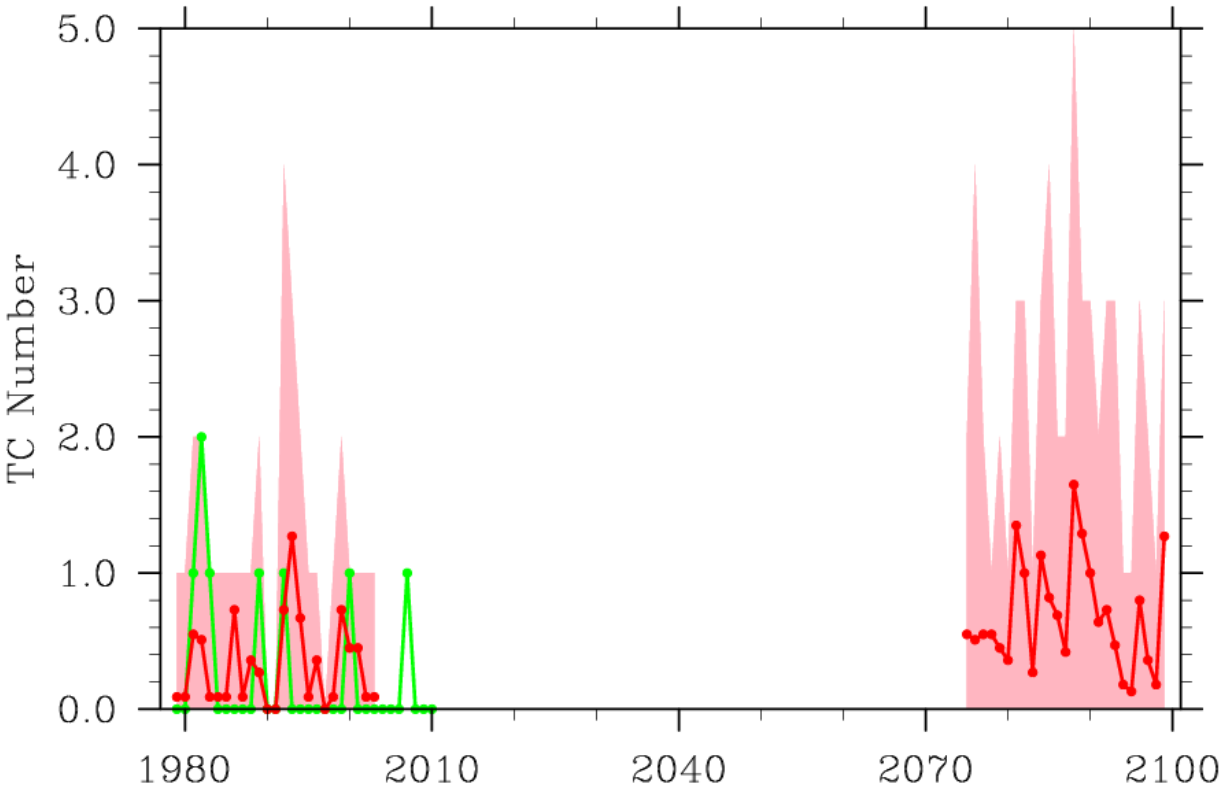

SUPPLEMENTARY FIGURE 1 Yearly variability in TC number approached coastal region around the Hawaiian Islands. The off-shore edges of the coastal region are defined as being 200 km from coast line of the Hawaiian Islands. The green line represents observations[18] (1979–2010), and the red lines are simulated ensemble mean of present-day experiments (1979–2003) and future experiments (2075–2099). The red shading represents the ensemble spread defined by minimum and maximum values of the ensemble experiments.

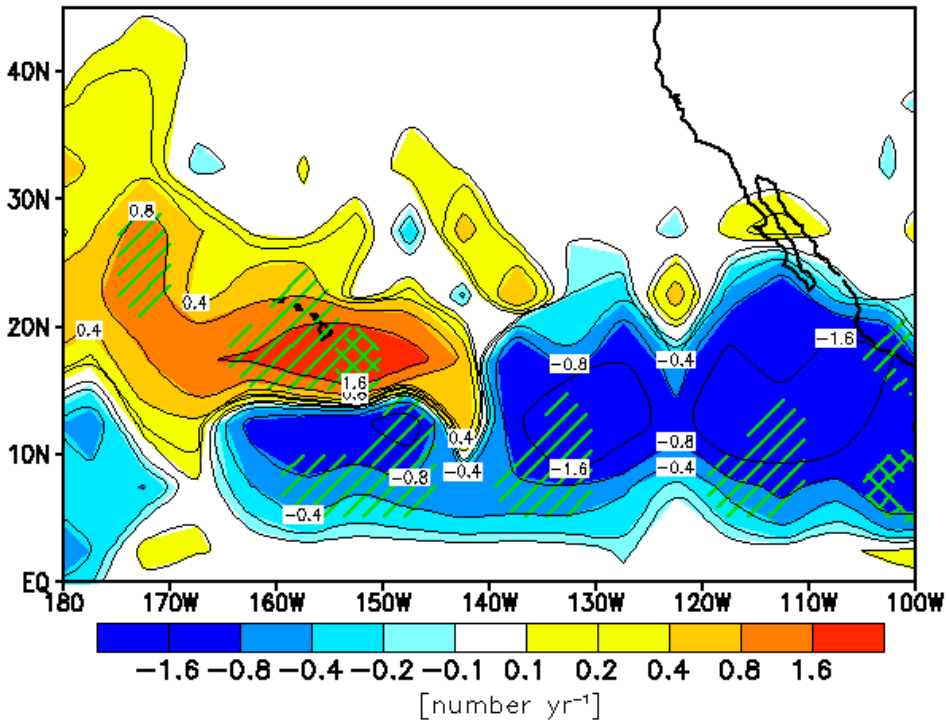

SUPPLEMENTARY FIGURE 2 Projected future change in annual mean of tropical cyclone frequency counted at every 5° × 5° grid cell for the idealized experiment with a uniform SST increase of 1.83°C. Single (crossed) green diagonal lines indicate statistical significance at the 90% (99%) confidence level according to the boot strap method.

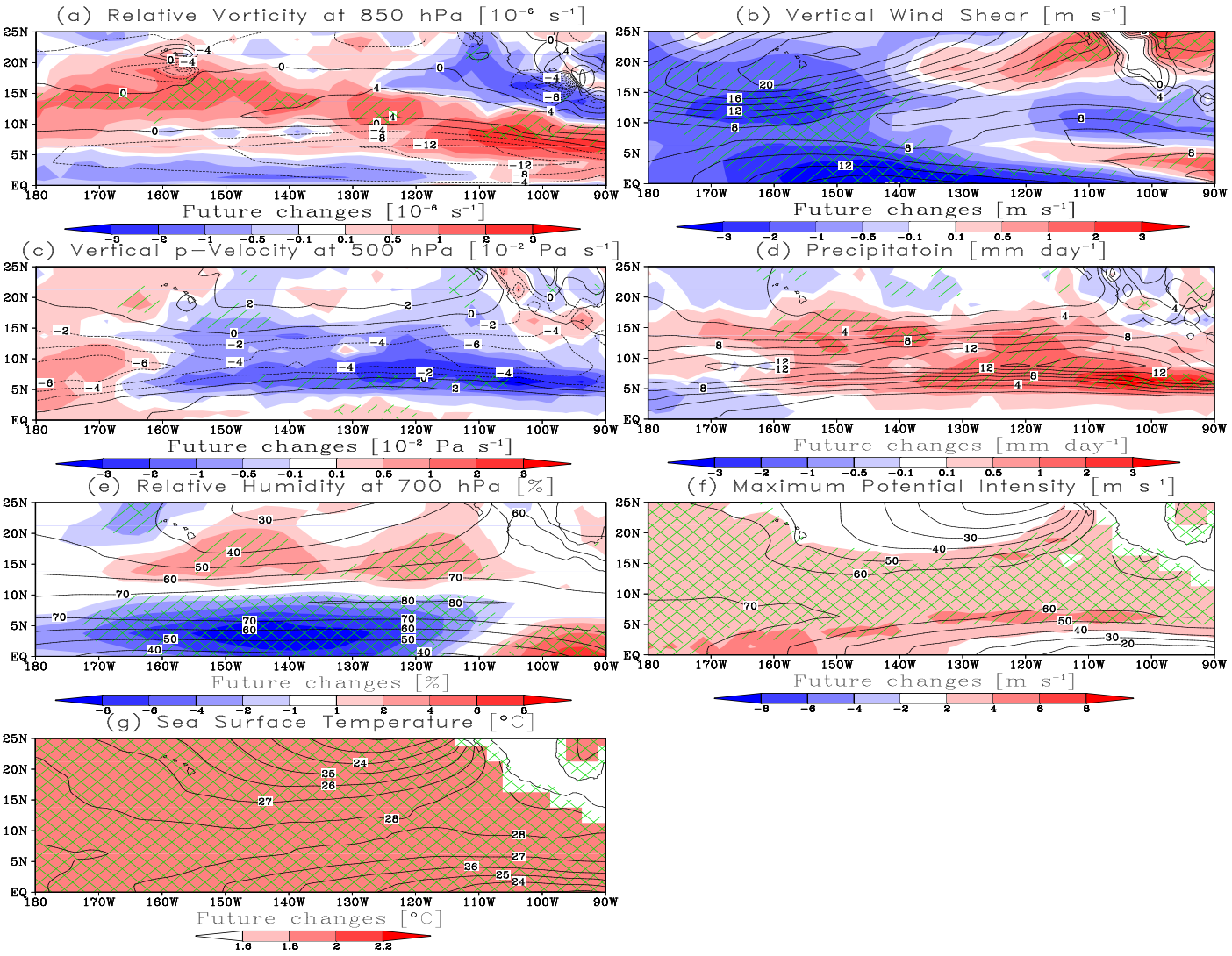

SUPPLEMENTARY FIGURE 3 Simulated changes in July–October mean large-scale variables from an additional experiment forced by a globally uniform change in SST of +1.83°C relative to the present-day (colour shading), and present-day mean (contours) for (a) relative vorticity at 850 hPa [10^{-6} s^{-1}], (b) vertical wind shear between 200 and 850 hPa [m s^{-1}], (c) vertical p-velocity at 500 hPa [10^{-2} Pa s^{-1}], (d) precipitation [mm day^{-1}], (e) relative humidity at 700 hPa [%], (f) maximum potential intensity [m s^{-1}], and (g) prescribed sea surface temperature [°C]. Single (crossed) green diagonal lines indicate statistical significance at the 90% (99%) confidence level by the boot strap method.

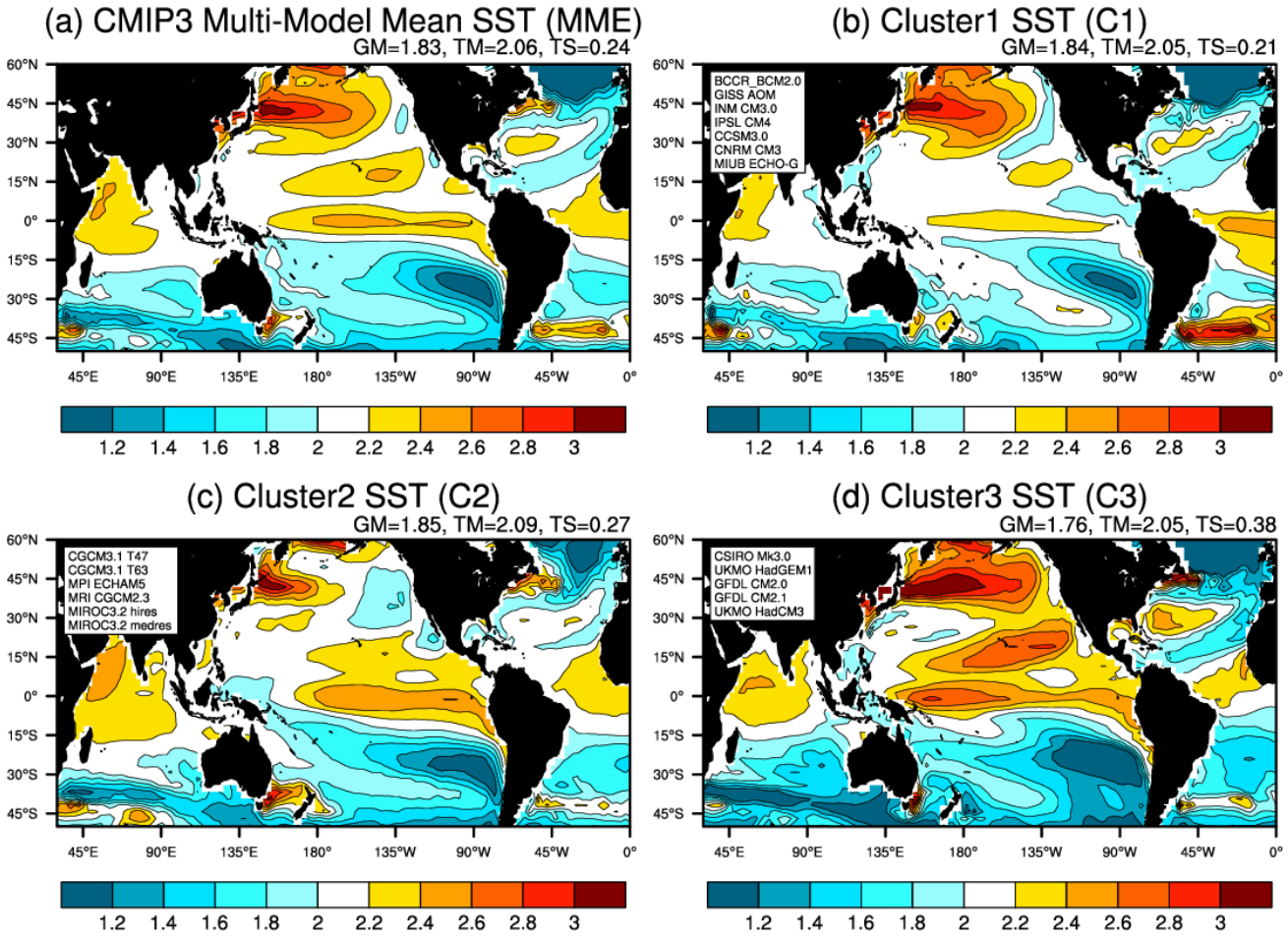

SUPPLEMENTARY FIGURE 4 Annual means of prescribed future changes in sea surface temperature (SST) [°C]. (a) Multi-model ensemble mean of 18 CMIP3 models (MME). (b)–(d) Changes in SST classified using a cluster analysis (C1–C3). The numbers at the top right of each panel show the global mean SST change (GM), tropical (30°S–30°N) mean SST change (TM), and standard deviation of the tropical SST spatial change (TS), respectively. The models listed in the top left corner of each panel are the CMIP3 models grouped in that cluster. Reprinted from ref. 1.

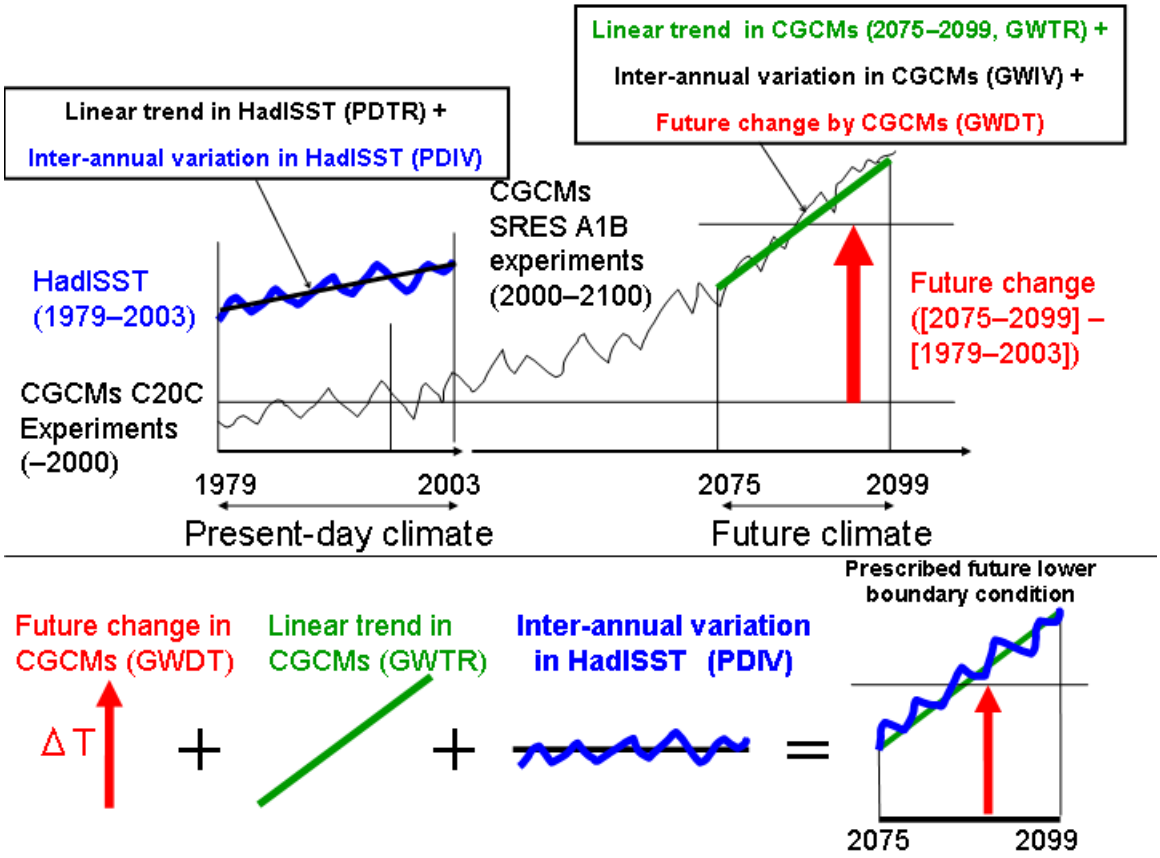

SUPPLEMENTARY FIGURE 5 Schematic diagram showing calculation of prescribed lower boundary conditions for the future projections. The abbreviations are as follows: SST (Sea Surface Temperature), HadISST (Hadley Centre observational SST), PDTR (trend in the present-day SST), PDIV (inter-annual variation in the present-day SST), GWTR (trend in the ensemble mean of future SSTs), GWIV (inter-annual variation in the ensemble mean of future SSTs), GWDT (averaged future changes in the ensemble mean of SSTs), CGCM (Coupled General Circulation Model), SRES (Special Report on Emission Scenarios), and C20C (Climate of the Twentieth Century). Reprinted from ref. 20.

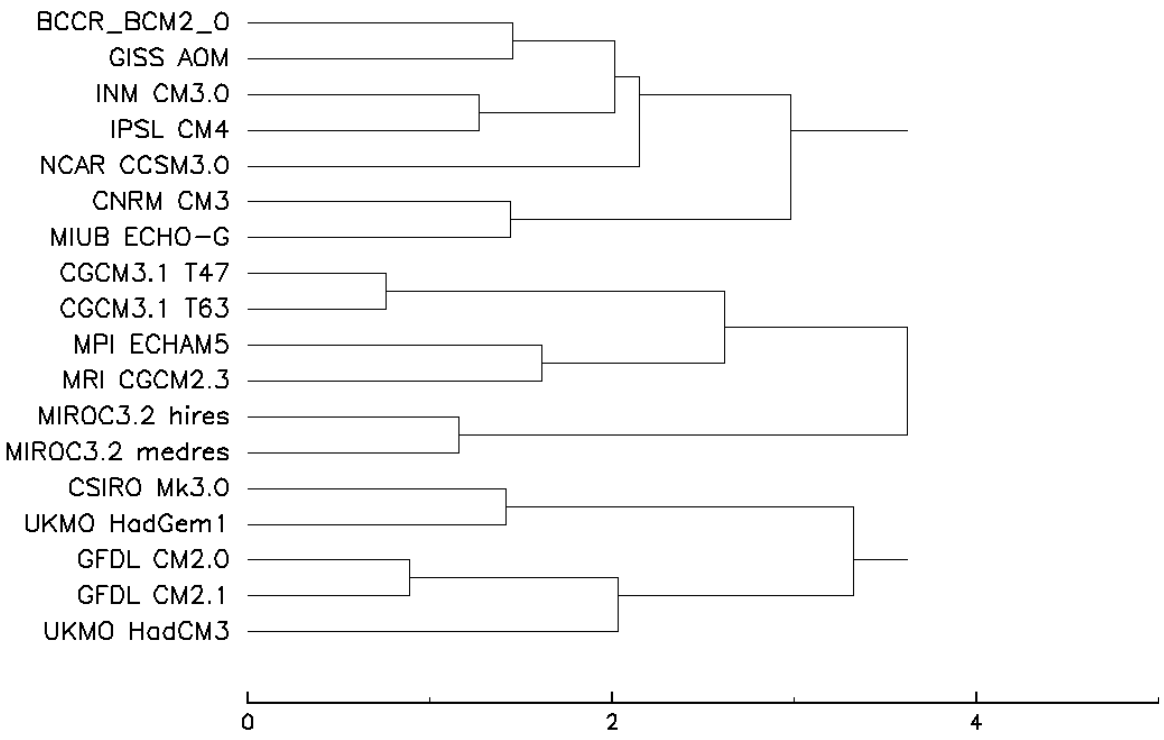

SUPPLEMENTARY FIGURE 6 Dendrogram for clustering of SSTs projected by the 18 CMIP3 models. The results of 15 clustering steps are indicated as the original 18 models are progressively joined from left to right in the diagram. The distances between joined clusters are indicated by the lengths of the horizontal lines. Reprinted from ref. 1.

Summary for Supplementary Information for

Projected future increase in tropical cyclones near Hawaii

Hiroyuki Murakami[1, 2], Bin Wang[2], Tim Li[2], and Akio Kitoh[1]

[1]Meteorological Research Institute, Tsukuba, Ibaraki, Japan

[2]Department of Meteorology and International Pacific Research Center,

University of Hawaii at Manoa, Honolulu, Hawaii 96822, USA

Nature Climate Change

Introduction

The file "supple.pdf" contains following information.

Supplementary Methods
Details in model description, experimental settings, and tropical cyclone detection method.

References
References used in the Supplementary Information.

Supplementary Table
Two tables for describing differences in the model versions and experiment design.

Supplementary Figure
Six figures for supporting the main text and experiment design.

Total file format is in PDF and file size is 4,200 KB.